https://doi.org/10.20575/00000061
Polar Data Journal, Vol. 9, 30–43, May 2025

Firn air composition at the H128 and NDFN sites, Dronning Maud Land, East Antarctica

Ikumi OYABU [1, 2]*, Kenji KAWAMURA [1, 2, 3], Kyotaro KITAMURA [1], Satoshi SUGAWARA [4], Shigeyuki ISHIDOYA [5], Taku UMEZAWA [6], Takuya SAITO [6], Daisuke GOTO [1, 2], Ryo FUJITA [7], Shinji MORIMOTO [8], Shuji AOKI [8] and Hideaki MOTOYAMA [1]

[1] National Institute of Polar Research, Research Organization of Information and Systems, 10-3, Midori-cho, Tachikawa, Tokyo 190-8518.
[2] Polar Science Program, Graduate Institute for Advanced Studies (SOKENDAI), 10-3, Midori-cho, Tachikawa, Tokyo 190-8518.
[3] Japan Agency for Marine-Earth Science and Technology, 2–15, Natsushima-cho, Yokosuka, Kanagawa 237-0061.
[4] Miyagi University of Education, 149 Aramaki Aza-Aoba, Aoba-ku, Sendai, Miyagi 980-0845.
[5] National Institute of Advanced Industrial Science and Technology (AIST), 16-1, Onogawa, Tsukuba, Ibaraki 305-8569.
[6] National Institute for Environmental Studies, 16-2, Onogawa, Tsukuba, Ibaraki 305-8506.
[7] Meteorological Research Institute, Japan Meteorological Agency, 1-1, Nagamine, Tsukuba, Ibaraki 305-0052.
[8] Graduate School of Science, Tohoku University, 6-3, Aramaki Aza-Aoba, Aoba-ku, Sendai, Miyagi 980-8578.
*Corresponding author. Ikumi Oyabu (oyabu.ikumi@nipr.ac.jp)
（Received October 30, 2024; Accepted February 12, 2025）

Abstract: Air sampled from polar firn is useful for reconstructing atmospheric composition over the last few decades and understanding the trapping processes of air in the ice sheets, as well as determining the age of air relative to the ice at the same depth. This paper presents the composition of firn air collected at H128 and NDFN in Dronning Maud Land, East Antarctica. The firn air at both sites was carefully sampled using a sampling system developed at the National Institute of Polar Research. We provide elemental and isotopic ratios of N_2, O_2, Ar, Kr, Xe, and Ne, as well as concentrations of CO_2, CH_4, N_2O, SF_6 and CFCs for both sites, measured using high-precision

measurement systems across multiple laboratories. The data would be valuable for studying air entrapment processes in firn and reconstructing past ice sheet environments and atmospheric compositions.

1. Background & Summary

Ice cores drilled at polar ice sheets contain ancient air, providing essential data for understanding past atmospheric composition and climate changes. Over time, snow accumulates on the ice sheets and gradually transforms into ice. Firn is the intermediate stage between snow and ice, with a typical depth of 40 to 120 m in the accumulation zone of ice sheets[1]. Air is transported through firn column by convection, advection and molecular diffusion, and eventually becomes permanently trapped as air bubbles in the ice at depths of approximately 10 to 15 m above the bottom of the firn. Consequently, the air in the ice sheets has been utilized to reconstruct past atmospheric compositions.

Firn air becomes progressively older with depth as it primarily travels by diffusion in the tortuous, open pores in the firn column. As a result, the firn itself serves as an archive of ancient air, preserving atmospheric records up to a century old[2]. This archive could bridge the gap between atmospheric records obtained from ice-core bubbles and direct modern observations. In addition, air composition is slightly altered by thermal and gravitational separations in the diffusive zone of the firn column, and relatively small gas molecules are fractionated during bubble formation in mass and size-dependent manners[3, 4]. Firn air thus helps to gain knowledge of how air composition fractionates within the firn and during the bubble formation, which is important for interpreting ice-core records. Firn air is also important for determining the gas age of the ice core. Because air is trapped at the bottom of the firn, the air enclosed in bubbles is younger than the surrounding ice matrix[5]. This age difference between air and ice at the same depth is called Δage, which may be estimated either directly from firn air data or through a combination of firn densification and firn-air transport models for which firn air data are used to constrain them.

In this paper, we present the depth profiles of various gas concentrations and isotopic ratios in firn at H128 and NDFN, located in Dronning Maud Land, East Antarctica (Fig. 1). The measured species include the isotopic and elemental ratios of N_2, O_2, Ar, Kr, Xe and Ne ($\delta^{29}N_2/^{28}N_2$, $\delta^{34}O_2/^{32}O_2$, $\delta O_2/N_2$, $\delta Ar/N_2$, $\delta^{40}Ar/^{36}Ar$, $\delta^{40}Ar/^{38}Ar$, $\delta^{38}Ar/^{36}Ar$, $\delta^{86}Kr/^{82}Kr$, $\delta^{86}Kr/^{83}Kr$, $\delta^{86}Kr/^{84}Kr$, $\delta^{132}Xe/^{129}Xe$, $\delta^{136}Xe/^{129}Xe$, $\delta^{136}Xe/^{132}Xe$, $\delta^{84}Kr/^{40}Ar$, $\delta^{132}Xe/^{40}Ar$, and $\delta^{22}Ne/^{40}Ar$), as well as concentrations of CO_2, CH_4, N_2O, SF_6, CFC-11, CFC-12, and CFC-113. Although firn air has been sampled at many polar sites over the past few decades[1], this is the first time that firn air data have been acquired for the H128 and NDFN sites. Moreover, few studies have measured noble gases in firn air samples. Therefore, our diverse datasets from the two locations in Antarctica with contrasting characteristics—one characterized by relatively high accumulation rates with strong winds and the other by low accumulation rates with calm conditions—are valuable for studying air fractionation and entrapment processes in firn, as well as reconstructing past ice sheet environments and atmospheric compositions.

2. Location

Firn air was sampled at H128 (69.393°N, 41.561°W, 1360 m above sea level) in January 2016 and NDFN (77.736°N, 39.118°W, 3772 m above sea level) in January 2019 (Fig. 1). For the H128 site, the surface density (0–1.92 m depths; observed in February 2016), mean accumulation rate (1992–2016), 10-m mean snow temperature (2016–2017), annual mean wind speed and annual mean pressure (2016–2017) are 339 kg m^{-3}, 13 cm w.e. yr^{-1}, -23.7 ˚C[8], 9.3 m s^{-1} (ref. 8) and 823 hPa[8], respectively. For the NDFN site, surface density (0–1 m depths; observed in December 2018) and mean accumulation rate (1992–2019) are 347 kg m^{-3} (ref. 6) and 2.46 cm w.e. yr^{-1} (ref. 7), respectively.

Automatic Weather Stations (AWSs) are installed at the H128 and NDF sites (~5 km south of NDFN, 77.788°N, 39.054°W, 3764 m above sea level). Although temperature and pressure were not measured at the NDFN sites, surface data at NDF are shown for reference, as NDF is only 5 km away from NDFN, and the surface environment should be similar. At NDF, surface density (0–1 m depths; observed in December 2017), mean accumulation rate (1992–2013 and 1992–2018), 10-m mean snow temperature (2018–2019), annual mean wind speed and annual mean pressure (2018–2019) at NDF are 357 kg m^{-3} (ref. 6, 7), 2.41 cm w.e. yr^{-1} (ref. 7), -56.9 ˚C, 3.6 m s^{-1} and 607 hPa[8], respectively. The AWS data are accessible at the National Institute of Polar Research (NIPR) ADS data repository[8].

3. Methods

Our sampling system was developed at NIPR based on the previous system by Kawamura *et al.*[9]. The basic concept of the system follows that of Schwander *et al.*[5]; however, the sampling method includes improvements introduced by Tohjima *et al.*[10] and Ishidoya *et al.*[11] to minimize isotope fractionation in atmospheric $\delta O_2/N_2$. A schematic of the sampling system is shown in Figure 2. The sampling system consists of a sealing device in the borehole, two boxes on the surface containing pumps and regulators, and the tubings that connect them. The sealing device consists of a bladder made from a 3-m-long natural rubber tube (3-mm wall thickness) with stainless steel flanges at both ends, a 6 mm O.D. tube (Dekabon polyethylene-aluminum composite tubing) to inflate the bladder, and two 10 mm O.D. tubes (Dekabon polyethylene-aluminum composite tubing) to purge and sample firn air. The bladder is used to isolate the bottom of the borehole from the overlying borehole and atmosphere. The depth range from the bottom of the borehole and the lower end of the seal is ~30 cm, and a stainless steel baffle plate[2, 3, 12] at ~10 cm above the borehole bottom separates the air intakes for the purge and sampling lines (Fig. 2). One of the boxes (purge box) contains an oil-free rocking piston pump (GAST, LOA) to inflate the bladder and purge the bottom of borehole. Another box (sampling box) is equipped with an air dryer (with magnesium perchlorate powder) and two pumps (KNF, N-145, and Senior Aerospace, MB-118 or MB-302) to sample firn air into a metal flask. The sample flasks are cylindrical in shape, made of stainless steel, and equipped with two all-metal and bellows-sealed manual valves (SS-4H) at each end, with a volume of about 1 L (NIPR flasks). We

also collected firn air into evacuated 6-L fused-silica-lined stainless steel canisters (SilcoCan, Restek Co. Ltd.) for halocarbon measurements at National Institute for Environmental Studies (NIES) (hereafter NIES flasks).

The sampling procedures are as follows. After drilling the firn to the planned sampling depth, the sealing system was lowered to the bottom of the borehole, and the bladder was inflated to isolate the air inlet from the overlying air in the borehole. The firn air was then withdrawn by both boxes to purge the bottom of the borehole, the inlet and the tubing at flow rates of 15 L min^{-1} (purge box) and ~12 L min^{-1} (sampling box) for more than 10 minutes. This procedure also flushes the sample flask. Next, the pressure in the sample flask was increased to ~+0.5 MPa (relative to the ambient pressure) by adjusting the back-pressure regulator, which reduced the flow rate to ~6 L min^{-1}. The pressurized flow was maintained for ~10 minutes. Finally, the two solenoid valves (SV2 and SV3) were closed simultaneously to stop the pressurized air flow through the sample flask, thereby minimizing isotope fractionation[11]. The firn air was then sampled by closing the four manual valves (MV4 to MV7), ensuring that the pressures between the outer and inner valves were the same as the flask pressure, minimizing fractionation in case of valve leakage. Caps with O-rings (Swagelok, VCO) were attached to each end of the flask. During the flushing, the CO_2 concentration of the firn air was monitored using a non-dispersive infrared analyzer (LI-COR, LI-840) to ensure sufficient purging.

To compare with firn air compositions, ground-level air sampling was also conducted. At H128, air was sampled at 0 m and 5.5 m above ground, while at NDFN, sampling was performed at 1.0 m and 1.5 m above ground. At H128, the tube connected to the MV1 of the sampling box was attached to a 5.5 m-long bamboo stick to collect air. At NDFN, the bladder with stainless steel flanges was supported by bamboo sticks set up in an X shape, and the air was collected using the same system as for firn air sampling. The valve operations for air collection were the same as those used for firn air sampling. At both sites, sampling was conducted approximately 50 m upwind from the firn air sampling locations.

The total number of air sampling depths, including surface air, was 20 for the NIPR flask and 13 for the NIES flask at the H128 site, and 27 for the NIPR flask and 25 for the NIES at the NDFN site. Air samples in two of the H128 NIES flasks were identified to be contaminated and the data were thus excluded.

Isotopic and elemental ratios of the N_2, O_2 ($\delta^{29}N_2/^{28}N_2$, $\delta^{34}O_2/^{32}O_2$, $\delta O_2/N_2$, $\delta Ar/N_2$) and noble gases ($\delta^{40}Ar/^{36}Ar$, $\delta^{40}Ar/^{38}Ar$, $\delta^{38}Ar/^{36}Ar$, $\delta^{86}Kr/^{82}Kr$, $\delta^{86}Kr/^{83}Kr$, $\delta^{86}Kr/^{84}Kr$, $\delta^{84}Kr/^{40}Ar$, $\delta^{132}Xe/^{40}Ar$, and $\delta^{22}Ne/^{40}Ar$) were measured at NIPR as follows. $\delta^{29}N_2/^{28}N_2$, $\delta^{34}O_2/^{32}O_2$, $\delta O_2/N_2$ and $\delta Ar/N_2$ were measured using a dual-inlet isotope ratio mass spectrometer (IRMS) (Thermo Fisher Scientific, Delta V) following established methods[13]. The isotopic and elemental ratios of Ar, Kr, Xe and Ne were measured using another dual-inlet IRMS (Thermo Fisher Scientific, MAT253). Isotopic and elemental ratios reported in this study were measured against reference gases in each laboratory and normalized against surface values. For NDFN firn air samples, $\delta^{132}Xe/^{129}Xe$, $\delta^{136}Xe/^{129}Xe$ and $\delta^{136}Xe/^{132}Xe$ were

also measured with the MAT253 using a separate aliquot of the air sample. The analytical method for the noble gases follows that described elsewhere[3, 14, 15] with slight modifications: a sample size of 80 mL, a gettering time of ~20 to 40 minutes at 900 ˚C and 10 minutes at 300 ˚C, and a homogenization time of more than 3 hours. For the IRMS measurements, the integration time and idle time are 16 or 8 s and 12 s for Ar isotopes and 26 s and 14 s for Kr and Xe isotopes, respectively. We run 4 blocks for each sample to obtain a total of 64 cycles for Ar isotopes, 4 blocks to obtain a total of 100 cycles for Kr isotopes, and 9 blocks to obtain a total of 225 cycles for Xe isotopes.

Isotopic and elemental ratios of the N_2, O_2 and Ar ($\delta^{29}N_2/^{28}N_2$, $\delta^{34}O_2/^{32}O_2$, $\delta^{40}Ar/^{36}Ar$, $\delta O_2/N_2$, $\delta Ar/N_2$) and CO_2 concentration for the H128 samples were also measured at National Institute of Advanced Industrial Science and Technology (AIST) using an IRMS (Thermo Fisher Scientific, Delta V) following established methods[16].

The CO_2, CH_4, N_2O and SF_6 concentrations in the NIPR flasks were measured at Tohoku University (TU) by using a non-dispersive infrared gas analyzer (NDIR; VIA-500R, HORIBA), a gas chromatograph (GC; Agilent 6890) equipped with a flame ionization detector (FID), and a GC equipped with an electron capture detector (ECD), respectively. Details for the measurements are described elsewhere[17, 18, 19, 20, 21]. SF_6 concentrations were also measured at Miyagi University of Education (MUE) by using a GC (Agilent 7890N) with an ECD[21]. The CO_2, CH_4, N_2O and SF_6 concentrations in some NIES flasks from the H128 site were also measured at TU (a total of 13 sampling depths). In addition, the CO_2 and CH_4 concentrations in the NIPR flasks from H128 were measured at NIPR using a GC (Agilent 7890A) with two FIDs[13]. Concentrations were determined against the TU2010-CO_2 scale for CO_2 (ref. 22), the TU1987-CH_4 scale for CH_4 (ref. 23, 24), the TU1991-N_2O scale for N_2O[25] and the TU2002-SF_6 scale for SF_6 (ref. 21), all of which are based on primary standard gases prepared gravimetrically. We note that the CH_4 concentrations were measured against the TU2008 scale, which was found to be about 3.0 ppb higher than the TU1987 scale[24]. The CH_4 measurement data were corrected accordingly to report on the TU1987 scale. The halocarbon concentrations in the NIES flasks were measured using a GC with a mass selective detector (MSD) based on the analytical method by Umezawa *et al.*[26]. Concentrations of individual halocarbons were determined against a working standard (compressed dry air) traceable to synthetic standards on the NIES-08 scales.

4. Data Records

Depth profiles of the firn air composition at H128 and NDFN are shown in Figure 3 and Figure 4, respectively. Flask number, depth, and gas data are provided as spreadsheets (.xlsx).

Depth profiles of densities at H128 and NDFN are shown in Figure 5. The NDFN density was previously published by Oyabu *et al.*[7] and is available at the NIPR ADS data repository[27]. For H128, the density data is provided in a spreadsheet format (.xlsx).

5. Technical Validation

The reproducibility of the laboratory measurements is assessed using the pooled standard deviation (SD) of replicates (measurements of two or more times) for each sample. The pooled SDs of $\delta^{29}N_2/^{28}N_2$, $\delta^{34}O_2/^{32}O_2$, $\delta O_2/N_2$ and $\delta Ar/N_2$ for the H128 samples measured at NIRP are 0.005 ‰, 0.007 ‰, 0.027 ‰ and 0.50 ‰, respectively. For the NDFN samples, the pooled SDs are 0.004 ‰, 0.008 ‰, 0.023 ‰ and 0.059 ‰, respectively. The reproducibility of $\delta^{29}N_2/^{28}N_2$, $\delta^{34}O_2/^{32}O_2$, $\delta^{40}Ar/^{36}Ar$, $\delta O_2/N_2$, $\delta Ar/N_2$, and CO_2 concentration measurements at AIST are estimated to be 0.002 ‰, 0.003 ‰, 0.013 ‰, 0.005 ‰, 0.008 ‰ and 0.2 ppm, respectively.

The pooled SDs of $\delta^{40}Ar/^{36}Ar$, $\delta^{40}Ar/^{38}Ar$, $\delta^{38}Ar/^{36}Ar$, $\delta^{86}Kr/^{82}Kr$, $\delta^{86}Kr/^{83}Kr$, $\delta^{86}Kr/^{84}Kr$, $\delta^{84}Kr/^{40}Ar$, $\delta^{132}Xe/^{40}Ar$, and $\delta^{22}Ne/^{40}Ar$ for the H128 samples are 0.005 ‰, 0.008 ‰, 0.006 ‰, 0.016 ‰, 0.019 ‰, 0.009 ‰, 0.146 ‰, 0.187 ‰, and 0.471 ‰, respectively. For the NDFN samples, the pooled SDs of $\delta^{40}Ar/^{36}Ar$, $\delta^{40}Ar/^{38}Ar$, $\delta^{38}Ar/^{36}Ar$, $\delta^{86}Kr/^{82}Kr$, $\delta^{86}Kr/^{83}Kr$, $\delta^{86}Kr/^{84}Kr$, $\delta^{132}Xe/^{129}Xe$, $\delta^{136}Xe/^{129}Xe$, $\delta^{136}Xe/^{132}Xe$, $\delta^{84}Kr/^{40}Ar$, $\delta^{132}Xe/^{40}Ar$, and $\delta^{22}Ne/^{40}Ar$ for the NDFN samples are 0.004 ‰, 0.007 ‰, 0.008 ‰, 0.015 ‰, 0.016 ‰, 0.010 ‰, 0.068 ‰, 0.150‰, 0.090 ‰, 0.057 ‰, 0.163 ‰, and 0.163 ‰, respectively.

The reproducibility of CO_2, CH_4, N_2O, and SF_6 measurements at TU and MUE are estimated to be 0.02 ppm, 2 ppb, 0.3 ppb, and 0.09 ppt, respectively. The reproducibility of CO_2 and CH_4 measured at NIPR is estimated to be 0.1 ppm and 1.5 ppb, respectively. The results of intercomparisons of the calibration scales with other international scales have been described elsewhere[13, 21, 28]. Note that the CO_2 concentrations for H128 from the NIPR flasks are significantly higher than the in-situ data and the NIES flask data (Fig. 3). It is suspected that the pre-treatment of the NIPR flasks for H128 was insufficient and caused CO_2 production in the flasks during the sample storage. Based on the experience, the pre-treatment for the NDFN flasks was made much longer (several months) at a higher temperature (up to 150°C), and storing tests were conducted in advance to confirm that no alteration would occur.

The measurement reproducibility of the halocarbon measurements was evaluated to be better than 1% for CFCs presented in this study.

6. Competing interests

The authors declare no competing interests.

7. Figures

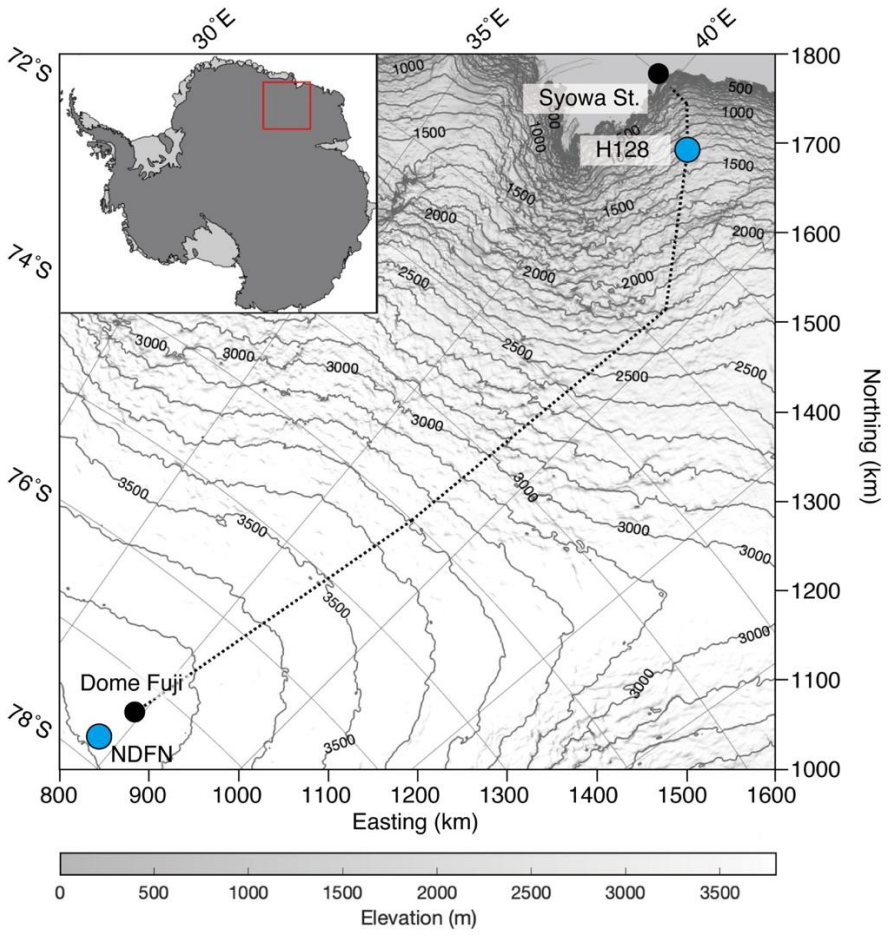

Figure 1. Locations of the H128 and NDFN firn-air sampling sites (blue circles) and Syowa and Dome Fuji stations (black circles). The black dotted line indicates the traverse route. Surface elevation contour intervals are 100 m (BedMachine[29]). Figures were drawn using an open-source MATLAB toolbox (Antarctic Mapping Tools[30]).

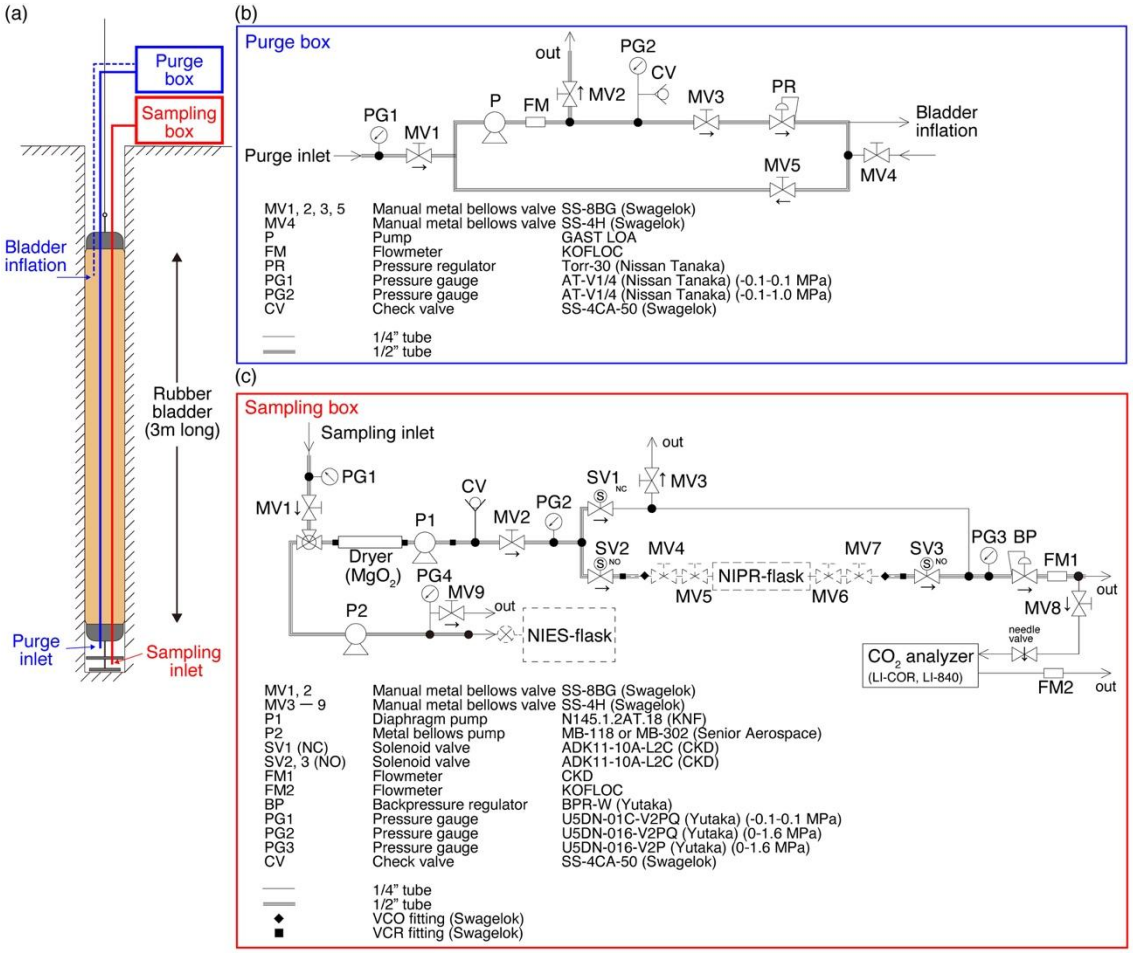

Figure 2. Schematic of (a) firn air sampling system, (b) purge box, and (c) sampling box.

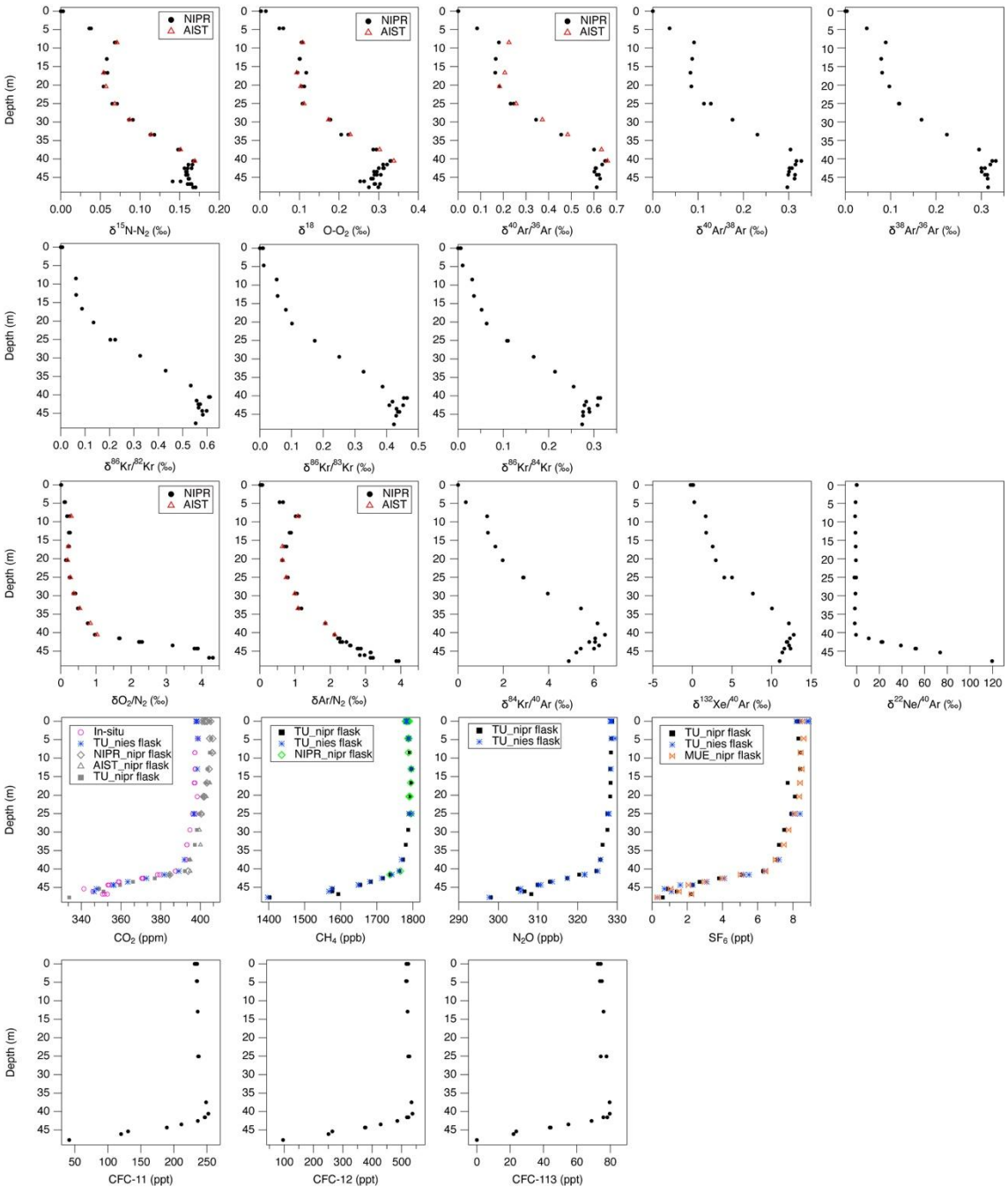

Figure 3. Depth profiles of measured gas species in firn at H128. Note that CO_2 concentrations from the NIPR flasks (grey markers) are significantly elevated by post-sampling artefacts, thus plotted here only for completeness.

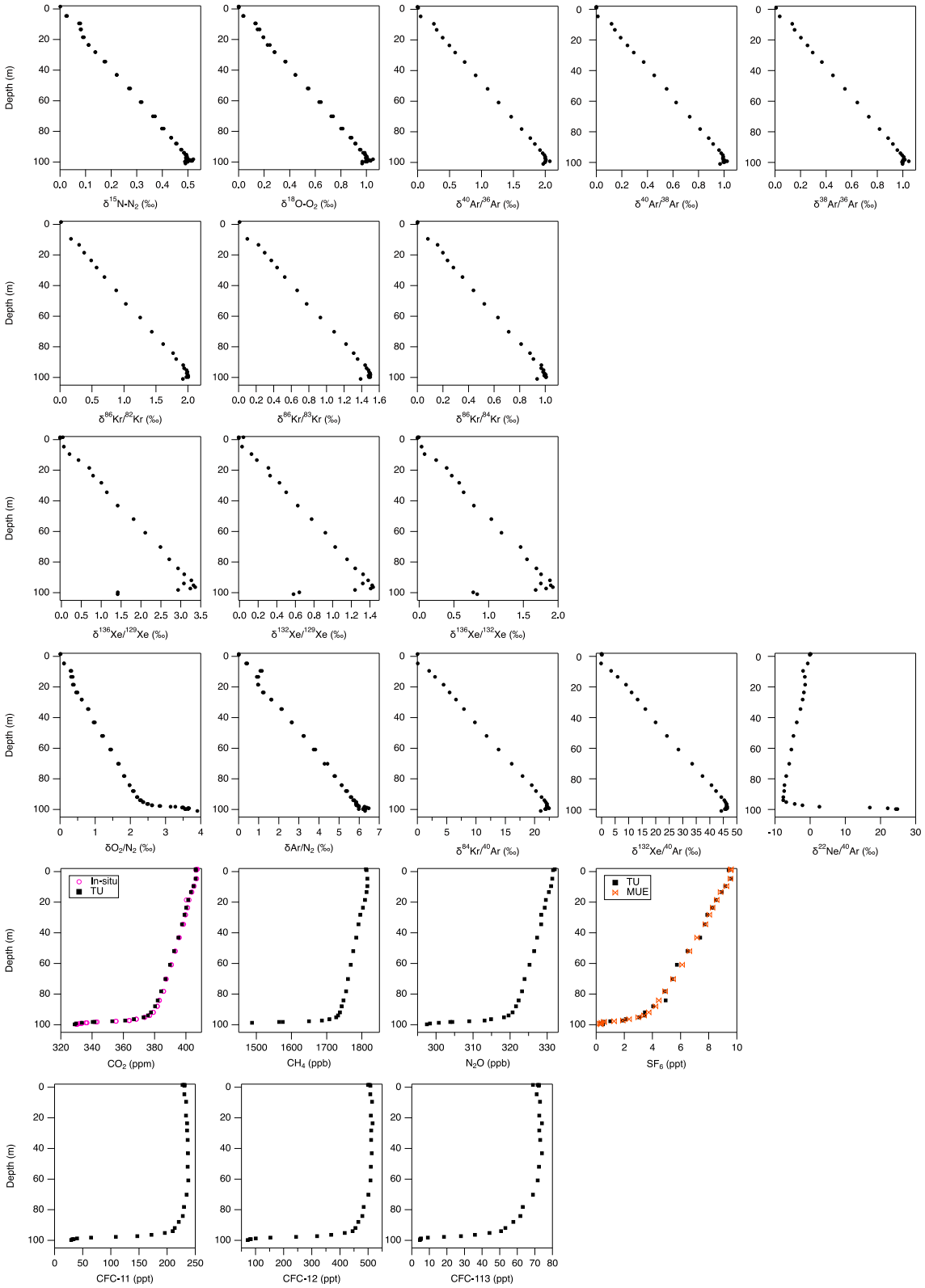

Figure 4. Depth profiles of measured gas species in firn at NDFN.

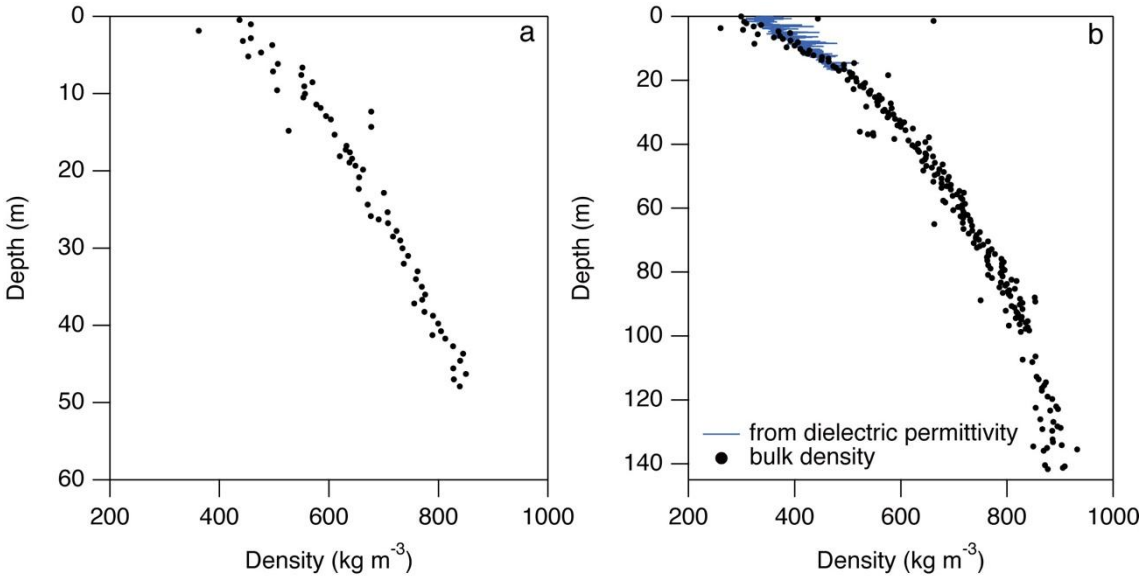

Figure 5. Depth profiles of density at (a) H128 and (b) NDFN[7].

Author contributions

KeK developed the sampling device with the support of KyK and IO. KyK, KeK, IO, DG and TS prepared the sample flasks. The shallow coring and firn air sampling at H128 were conducted by KeK and HM, and those at NDFN were conducted by KeK. IO and KyK measured isotopic and elemental ratios of N_2, O_2 and noble gases at NIPR. SI measured isotopic and elemental ratios of N_2, O_2 and Ar, and CO_2 concentration at AIST. IO, KeK, SS, SM and RF measured CO_2, CH_4 and N_2O concentrations at TU. SS measured SF_6 concentrations at MUE. SM and SA maintained the measurement systems and the calibration scales at TU. TU and TS measured CFC concentrations at NIES. IO wrote the manuscript with contributions from all co-authors.

Acknowledgments

We acknowledge the members of the Japanese Antarctic Research Expedition who contributed to the traverse and firn air sampling. This study was supported by JSPS and MEXT KAKENHI (Grant Numbers JP24K03070 to IO, JP17H06320, JP24H00762 and JP24H02345 to KK, JP23H00513 to SS, JP22H05006 to SI, JP17K18342 to TU), by JST FOREST Program (Grant Number JPMJFR216X to IO) and by NIPR Research Projects (Advanced Project and KP305).

References

1. Buizert, C. Firn air processes in ice core science. Encyclopedia of Quaternary Science (Third Edition). 2025, 3, p. 105–121. https://doi.org/10.1016/B978-0-323-99931-1.00092-1.
2. Battle, M. et al. Atmospheric gas concentrations over the past century measured in air from firn at the South Pole. Nature. 1996, 383, p. 231–235. https://doi.org/10.1038/383231a0.
3. Severinghaus, J. P. and Battle, M. O. Fractionation of gases in polar ice during bubble close-off: New constraints from firn air Ne, Kr and Xe observations. Earth Planet. Sci. Lett. 2006, 244 (1-2), p. 474–500. https://doi.org/10.1016/j.epsl.2006.01.032.
4. Battle, M. O. et al. Controls on the movement and composition of firn air at the West Antarctic Ice Sheet Divide. Atmos. Chem. Phys. 2011, 11 (21), p. 11007-11021. https://doi.org/10.5194/acp-11-11007-2011.
5. Schwander, J. et al. The Age of the Air in the Firn and the Ice at Summit, Greenland. Journal of Geophysical Research: Atmospheres. 1993, 98 (D2), p. 2831–2838. https://doi.org/10.1029/92JD02383.
6. Inoue, R. et al. Spatial distribution of vertical density and microstructure profiles in near-surface firn around Dome Fuji, Antarctica. The Cryosphere. 2024, 18 (1), p. 425–449. https://doi.org/10.5194/tc-18-425-2024.
7. Oyabu, I. et al. Temporal variations of surface mass balance over the last 5000 years around Dome Fuji, Dronning Maud Land, East Antarctica. Clim. Past. 2023, 19 (2), p. 293–321. https://doi.org/10.5194/cp-19-293-2023.
8. Motoyama, H. et al., 2019, Automatic Weather Station on Antarctic ice sheet, 1.00, Arctic Data archive System (ADS), Japan, https://ads.nipr.ac.jp/dataset/A20190524-003.
9. Kawamura, K. et al. Convective mixing of air in firn at four polar sites. Earth Planet. Sci. Lett. 2006, 244 (3-4), p. 672–682. https://doi.org/10.1016/j.epsl.2006.02.017.
10. Tohjima, Y., Mukai, H., Machida, T., and Nojiri, Y. Gas-chromatographic measurements of the atmospheric oxygen/nitrogen ratio at Hateruma Island and Cape Ochi-ishi, Japan. Geophys. Res. Lett. 2003, 30 (12), 1653. https://doi.org/10.1029/2003GL017282.
11. Ishidoya, S. et al. Ship-based observations of atmospheric potential oxygen and regional air-sea O_2 flux in the northern North Pacific and the Arctic Ocean. Tellus B: Chemical and Physical Meteorology. 2016, 68 (1), 29972. https://doi.org/10.3402/tellusb.v68.29972.
12. Bender, M. L., Tans, P. P., Ellis, J. T., Orchardo, J., and Habfast, K. A high precision isotope ratio mass spectrometry method for measuring the O_2/N_2 ratio of air. Geochim. Cosmochim. Acta. 1994, 58 (21), p. 4751–4758. https://doi.org/10.1016/0016-7037(94)90205-4.
13. Oyabu, I. et al. New technique for high-precision, simultaneous measurements of CH_4, N_2O and CO_2 concentrations; isotopic and elemental ratios of N_2, O_2 and Ar; and total air content in ice cores by wet extraction. Atmos. Meas. Tech. 2020, 13 (12), p. 6703–6731. https://doi.org/10.5194/amt-13-6703-2020.
14. Severinghaus, J. P., Grachev, A., Luz, B., and Caillon, N. A method for precise measurement of argon 40/36 and krypton/argon ratios in trapped air in polar ice with applications to past firn thickness and

abrupt climate change in Greenland and at Siple Dome, Antarctica. Geochim. Cosmochim. Acta. 2003, 67 (3), p. 325–343. https://doi.org/10.1016/S0016-7037(02)00965-1.

15. Kawamura, K. et al. Kinetic fractionation of gases by deep air convection in polar firn. Atmos. Chem. Phys. 2013, 13 (21), p. 11141–11155. https://doi.org/10.5194/acp-13-11141-2013.
16. Ishidoya, S. and Murayama, S. Development of a new high precision continuous measuring system for atmospheric O_2/N_2 and Ar/N_2 and its application to the observation in Tsukuba, Japan. Tellus B. Chemical and Physical Meteorology. 2014, 66 (1), 22574. https://doi.org/10.3402/tellusb.v66.22574.
17. Nakazawa, T., Morimoto, S., Aoki, S., and Tanaka, M. Time and space variations of the carbon isotopic ratio of tropospheric carbon dioxide over Japan. Tellus B. Chemical and Physical Meteorology. 1993, 45 (3), p. 258–274. https://doi.org/10.3402/tellusb.v45i3.15728.
18. Morimoto, S., Nakazawa, T., Higuchi, K., and Aoki, S. Latitudinal distribution of atmospheric CO_2 sources and sinks inferred by $\delta^{13}C$ measurements from 1985 to 1991. Journal of Geophysical Research: Atmospheres. 2000, 105 (D19), p. 24315–24326. https://doi.org/10.1029/2000JD900386.
19. Umezawa, T. et al. Variations of tropospheric methane over Japan during 1988–2010. Tellus B. Chemical and Physical Meteorology. 2014, 66 (1), 23837. https://doi.org/10.3402/tellusb.v66.23837.
20. Ishijima, K. et al. Temporal variations of the atmospheric nitrous oxide concentration and its $\delta^{15}N$ and $\delta^{18}O$ for the latter half of the 20th century reconstructed from firn air analyses. Journal of Geophysical Research: Atmospheres. 2007, 112, D03305. https://doi.org/10.1029/2006JD007208.
21. Sugawara, S. et al. Age and gravitational separation of the stratospheric air over Indonesia. Atmos. Chem. Phys. 2018, 18 (3), p. 1819–1833. https://doi.org/10.5194/acp-18-1819-2018.
22. Goto, D., Morimoto, S., Ishidoya, S., Aoki, S., and Nakazawa, T. Terrestrial biospheric and oceanic CO_2 uptakes estimated from long-term measurements of atmospheric CO_2 mole fraction, $\delta^{13}C$, and $\delta(O_2/N_2)$ at Ny-Ålesund, Svalbard. Journal of Geophysical Research Biogeosciences. 2017, 122 (5), p. 1192–1202. https://doi.org/10.1002/2017JG003845.
23. Aoki, S., Nakazawa, T., Murayama, S., and Kawaguchi, S. Measurements of atmospheric methane at the Japanese Antarctic Station, Syowa. Tellus B: Chemical and Physical Meteorology. 1992, 44 (4), p. 273–281. https://doi.org/10.3402/tellusb.v44i4.15455.
24. Fujita, R. et al. Temporal Variations of the Mole Fraction, Carbon, and Hydrogen Isotope Ratios of Atmospheric Methane in the Hudson Bay Lowlands, Canada. Journal of Geophysical Research: Atmospheres. 2018, 123 (9), p. 4695–4711. https://doi.org/10.1002/2017JD027972.
25. Machida, T., Nakazawa, T., Fujii, Y., Aoki, S., and Watanabe, O. Increase in the atmospheric nitrous oxide concentration during the last 250 years. Geophys. Res. Lett. 1995, 22 (21), p. 2921–2924. https://doi.org/10.1029/95GL02822.
26. Umezawa, T. et al. Towards reconstructing the Arctic atmospheric methane history over the 20th century: measurement and modelling results for the North Greenland Ice Core Project firn. Atmos. Chem. Phys. 2022, 22 (10), p. 6899–6917. https://doi.org/10.5194/acp-22-6899-2022.
27. Oyabu, I. et al., 2023, Accumulation rate, volcanic tie points, ECM, DEP, nssSO4, density and

chronology from shallow ice cores around Dome Fuji, East Antarctica, 1.00, Arctic Data archive System (ADS), Japan, https://doi.org/10.17592/001.2022081901.

28. Global Monitoring Laboratory Earth System Research Laboratories. “WMO/IAEA Round Robin Comparison Experiment”. https://www.esrl.noaa.gov/gmd/ccgg/wmorr/ (accessed 2024-10-20).
29. Morlighem, M. et al. Deep glacial troughs and stabilizing ridges unveiled beneath the margins of the Antarctic ice sheet. Nat. Geosci. 2020, 13, p. 132–137. http://doi.org/10.1038/s41561-019-0510-8.
30. Greene, C. A., Gwyther, D. E., and Blankenship, D. D. Antarctic Mapping Tools for Matlab. Computers & Geosciences. 2017, 104, p. 151–157. https://doi.org/10.1016/j.cageo.2016.08.003.

Data Citations

Oyabu, I., Kawamura, K., Kitamura, K., Sugawara, S., Ishidoya, S., Umezawa, T., Saito, T., Goto, D., Fujita, R., Morimoto, S., Aoki, S., and Motoyama, H. Elemental and isotopic compositions of N_2, O_2, and noble gases, and concentrations of greenhouse gases and halocarbons in firn air at H128 and NDFN, Dronning Maud Land, East Antarctica. 1.20, Japan, Arctic Data archive System (ADS), 2025. https://doi.org/10.17592/001.2024102102